
Reconstruct-and-Generate Diffusion Model for Detail-Preserving Image Denoising

Yujin Wang*

Shanghai Artificial Intelligence Laboratory
wangyujin@pjlab.org.cn

Lingen Li

The Chinese University of Hong Kong
lgli@link.cuhk.edu.hk

Tianfan Xue

The Chinese University of Hong Kong
tfxue@ie.cuhk.edu.hk

Jinwei Gu

The Chinese University of Hong Kong
jwgu@cuhk.edu.hk

Abstract

Image denoising is a fundamental and challenging task in the field of computer vision. Most supervised denoising methods learn to reconstruct clean images from noisy inputs, which have intrinsic spectral bias and tend to produce over-smoothed and blurry images. Recently, researchers have explored diffusion models to generate high-frequency details in image restoration tasks, but these models do not guarantee that the generated texture aligns with real images, leading to undesirable artifacts. To address the trade-off between visual appeal and fidelity of high-frequency details in denoising tasks, we propose a novel approach called the Reconstruct-and-Generate Diffusion Model (RnG). Our method leverages a reconstructive denoising network to recover the majority of the underlying clean signal, which serves as the initial estimation for subsequent steps to maintain fidelity. Additionally, it employs a diffusion algorithm to generate residual high-frequency details, thereby enhancing visual quality. We further introduce a two-stage training scheme to ensure effective collaboration between the reconstructive and generative modules of RnG. To reduce undesirable texture introduced by the diffusion model, we also propose an adaptive step controller that regulates the number of inverse steps applied by the diffusion model, allowing control over the level of high-frequency details added to each patch as well as saving the inference computational cost. Through our proposed RnG, we achieve a better balance between perception and distortion. We conducted extensive experiments on both synthetic and real denoising datasets, validating the superiority of the proposed approach.

1 Introduction

Image denoising is a fundamental problem in computational photography, with wide applications in medical imaging, remote sensing, computer vision, and more. DNN-based reconstructive image denoising methods [12; 52; 45; 51] learn to reconstruct clean images from noisy observation, which are promising but intrinsically tend to produce blurry images due to their spectral bias [38; 49] and the ill-posed nature of the denoising problem. Recent advances in generative models [21; 4; 16] have demonstrated the great potential of preserving high-frequency details in the denoising process. Generative methods improve visual perception by decorating noisy areas with generated high-frequency textures. However, this improvement comes at the cost of fidelity loss. Researchers have observed that these methods occasionally introduce undesired new textures that are unrelated to the original clean images, resulting in high-frequency artifacts [33]. In Figure 1, we can see an example where the generative model, Latent Diffusion Model (LDM), produces a denoised output

*Corresponding author

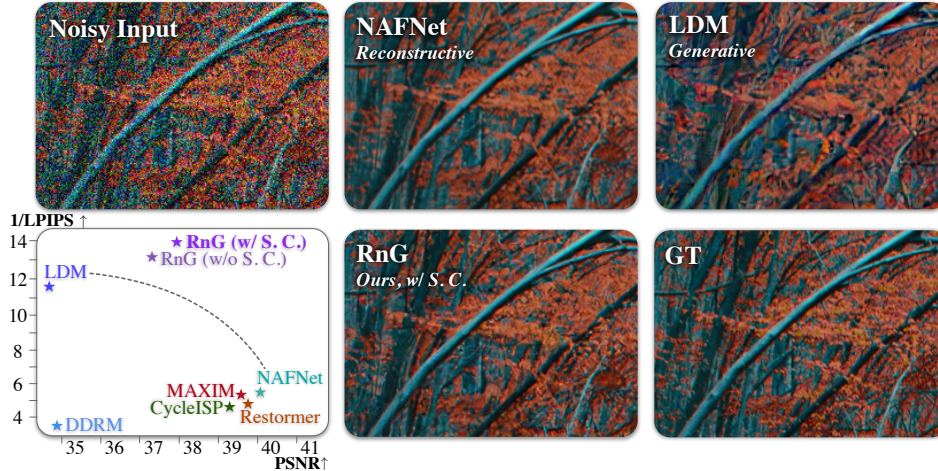


Figure 1: In this work, we proposed a Reconstructive-and-Generative (RnG) denoising model, that achieves the best trade-off between perception (measured by LPIPS) and distortion (measured by PSNR) as shown on the left. The visual result also indicates the proposed RnG produces detail-preserved denoising results. On the contrary, the reconstructive method, like NAFNet, often generates over-smoothed results (shown on the right). The generative method on the other side, sometimes outputs artificial textures that are not consistent with ground truth. The *S.C.* is short for step controller of the proposed RnG.

with textures that significantly deviate from the ground truth. The perception-distortion trade-off curve is proposed to describe this phenomenon, and the performance of current state-of-the-art methods can be plotted as a curve that represents the current perception-distortion trade-off frontier, as shown in the bottom-left part of Figure 1.

Given the considerable performance of reconstructive and generative methods in distortion and perception metrics, respectively, can we further push the boundary of the current perception-distortion curve by harnessing the strengths of both approaches?

To this point, we propose a novel reconstruct-and-generate diffusion model (RnG) for detail-preserving image denoising, which contains a reconstructive module and a generative module, leveraging the strengths of both two types of methods. Its reconstructive module produces an initial estimation that recovers low-frequency clean images with high fidelity. This initial estimation is then enhanced by the generative module, a conditional diffusion model, to include additional residual high-frequency details. Additionally, the reconstructive module can be any DNN-based denoiser, and the NAFNet is proven to be the best candidate in our experiments. The proposed RnG diffusion model addresses the fidelity problem in common generative methods used for image-denoising tasks like DDRM and LDM, pushing the limit of the current perception-distortion curve a step forward.

Furthermore, we recognize that in some cases, such as images with simple textures like the sky, the initial estimation is already visually satisfactory, and further generated texture may actually introduce artifacts to the final result. As high-frequency details are incrementally injected during the iterative sampling and denoising process, it is possible for us to limit the generated high-frequency details when necessary. Therefore, we introduce a step controller that controls the generation process by predicting the sampling step of the diffusion model for each input patch to avoid undesirable artifacts, improving perceptual performance and avoiding meaningless computational costs. Extensive experiments demonstrate that the proposed RnG outperforms existing state-of-the-art models on multiple perceptual metrics with real and synthetic denoising datasets, achieving superior visual quality.

Our main contributions can be summarized as follows:

- We proposed the Reconstruct-and-Generate Diffusion Model, which alleviates the fidelity problem of generative denoising methods and conveniently achieves better perceptual quality, leading to a better trade-off between perception and distortion.

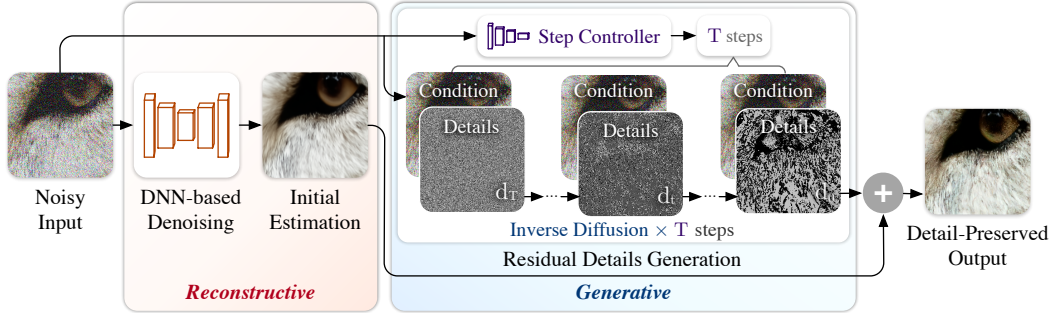


Figure 2: The proposed RnG consists of two key components: the reconstructive module, which utilizes a DNN-based denoiser, and the generative module, which generates residual details in inverse diffusion. The reconstructive module produces an initial estimation from the noisy input, while the generative module generates residual details conditioned on the noisy input. To further enhance perceptual performance, an additional step controller takes the noisy image as input and predicts the optimal number of inverse diffusion steps. This step controller effectively controls the generation intensity and prevents the occurrence of undesirable artifacts.

- We proposed an adaptive step controller to control the generation intensity of the RnG based on the observation that the increasing step in diffusion may lead to artifact, making the proposed RnG flexible to different inputs without any expensive retraining or fine-tuning on the diffusion model itself and further achieving higher perceptual quality and less distortion.
- Our approach enables us to expedite the inference of diffusion-based models by utilizing initial predictions and a step controller to reduce the number of diffusion inference steps.

2 Related Work

Traditional image denoising methods are often based on image priors [3; 17; 19; 8; 14; 15; 18; 22]. With the development of deep neural networks (DNNs), data-driven denoising methods achieved significant advances [25]. DnCNN [53] is one of the widely used convolutional denoising networks. Following DnCNN, many different network architectures were designed based on convolutional neural network (CNN) [12; 52; 45] and Transformer [31; 51]. Those methods usually adopt pixel-wise loss as a straightforward training objective and optimize the denoising model to achieve high performance in PSNR (peak signal-to-noise ratio). However, the well-known phenomenon perception-distortion trade-off [6] indicates that PSNR and other distortion metrics only partially correspond to human perception, and high distortion metrics are usually accompanied by lower perceptual quality.

In addition to supervised denoising approaches, there are studies that concentrate on using unsupervised denoising methods to circumvent the need for collecting noisy-clean training pairs. One approach to unsupervised denoising involves generating training pairs using a generative adversarial network (GAN) [11; 9]. Another approach is to train a neural network solely on noisy input images [5; 48; 29; 30; 37]. Although no paired data is required for training, existing unsupervised denoising methods still exhibit noticeable performance gaps compared to their supervised counterparts [36]. Therefore, in this work, we focus on supervised denoising.

Recently, diffusion model [23; 44; 43] has achieved state-of-the-art perceptual results in the field of image generation. There are also novel approaches [28; 27] for handling the image denoising task using diffusion models by samples from the posterior distribution given the noisy image. Diffusion models are employed in other restoration tasks [41; 47; 39; 40] to solve the image inverse problem. However, it is widely observed that diffusion models usually report lower distortion metrics [41; 47], such as PSNR, than other non-generative approaches, indicating their lack of fidelity in image restoration tasks.

3 Reconstruct-and-Generate Diffusion Model

In this section, we will introduce the RnG, which consists of the reconstructive module and generative module, whose framework is illustrated in Figure 2. The RnG combines the merit of the reconstructive denoising method, which maintains the fidelity of the output images, and the advantage of the generative method, which preserves high-frequency details.

Specifically, given a noisy image x_i , the corresponding clean image y_i , the reconstructive module employs a DNN-based denoiser r_θ to produce the initial estimation $r_\theta(x_i)$ from the noisy image, where θ are learnable model weights. In addition, the generative module employs a diffusion model g_θ to learn the condition distribution $P(y_i - r_\theta(x_i)|x_i)$ and outputs the MAP (Maximum A Posteriori Estimation) result, denoted as $g_\theta(x_i)$. The final denoising output is the summation of the two parts, which is denoted as $r_\theta(x_i) + g_\theta(x_i)$. Figure 2 summarizes the overall workflow of our method.

Compared to previous diffusion models [39; 41], one important difference of the diffusion model used in our generative module is that our model only learns a conditional distribution of residual details given the noisy image. There are two advantages of this design. Firstly, the reconstructive denoising model can recover the majority of low-frequency components but may wipe out some high-frequency details, whereas the generative diffusion model can help. Secondly, current diffusion models for denoising directly learn to generate clean images from noisy observations without any initial estimation [39; 41], which requires the diffusion model to learn both the faithful low-frequency and the high-frequency components. On the contrary, the generative module of our proposed model focuses on learning the high-frequency details only and leaves the prediction of the low-frequency component to the reconstructive module. Since the reconstructive module has higher fidelity, our approach can reduce the possibility of the diffusion model producing artifacts that deviate from target clean images.

In the following, we will first give a quick overview of the generative diffusion model and then introduce our step controller, training scheme, and optimization targets.

3.1 Generative Model

Our denoising training dataset consists of noisy-clean image pairs $\{x_i, y_i\}_{i=1}^N$. To train our models, we first generate noisy-detail data pairs $\{x_i, d_i\}_{i=1}^N$, where $d_i = y_i - r_\theta(x_i)$. We then train a denoising diffusion probabilistic (DDPM) model [42; 23] that estimates details d_i given the denoising output of the reconstructive model $r_\theta(x_i)$.

Following the classic diffusion process setup, we define a forward Markovian diffusion process q that gradually adds Gaussian noise to a clean residual detail image d_0 over T iterations:

$$q(d_t | d_{t-1}) = \mathcal{N}(d_t | \sqrt{\alpha_t} d_{t-1}, (1 - \alpha_t)\mathbf{I}), \quad (1)$$

where $\alpha_t \in (0, 1)$ for all $t = 1, \dots, T$ and controls the variance of noise added at each step. To model the posterior distribution $p(d_{t-1}|d_0, d_t)$, we use the reparameterization trick to train a denoising network g_θ by minimizing the variational lower bound. Specifically, we take noise level ($\gamma_t = \prod_{i=1}^t \alpha_i$) as input to the denoising model g_θ , similar to [13; 43; 47; 41]. Please refer to the supplementary material for the detailed structure of g_θ . And training the model by minimizing this objective function:

$$\mathbb{E} \left\| \epsilon - g_\theta(\sqrt{\gamma_t} d_0 + \sqrt{1 - \gamma_t} \epsilon, \gamma_t, x) \right\|_p^p, \quad (2)$$

where $\epsilon \sim \mathcal{N}(0, I)$ is the Gaussian noise added at each step, x is a noisy image from the training dataset, and d_0 is the residual high-frequency detail data obtained by $d_0 = y - r_\theta(x)$.

The inference process is defined as a reverse Markovian process starting from Gaussian noise d_T , and iterative infers d_t as:

$$d_{t-1} \leftarrow \frac{1}{\sqrt{\alpha_t}} \left(d_t - \frac{1 - \alpha_t}{\sqrt{1 - \gamma_t}} g_\theta(x, d_t, \gamma_t) \right) + \sqrt{1 - \alpha_t} \epsilon_t, \quad (3)$$

where $\epsilon \sim \mathcal{N}(0, I)$. Detailed derivation of Equations 2 and 3 will be presented in the supplementary material.

In the inference stage, we conduct a small grid search over the noise schedule hyper-parameters and select the model with the best LPIPS score [55], similar to [47]. We note that this inference-time hyper-parameter tuning is relatively free because it does not require retraining or finetuning the model itself.

3.2 Step Controller

To further reduce potential artifacts introduced by the generative diffusion process, we have developed a diffusion step control module that determines the optimal amount of high-frequency details to be injected into the final output. For many smooth regions like the sky, the initial estimation of the

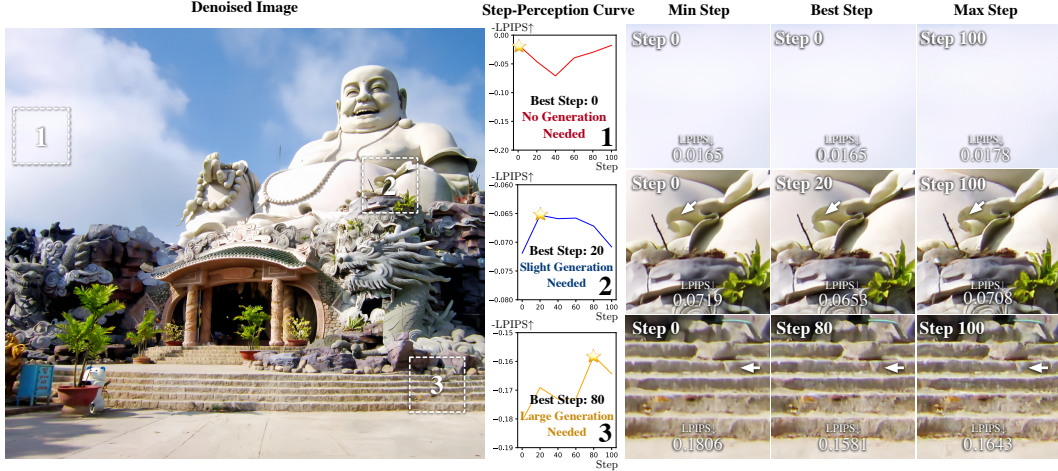


Figure 3: Illustration of patches generated in best diffusion steps that are searched towards better LPIPS and three selected patches generated in min (the zero step, which is equivalent to generating nothing), best, and max steps. As we can see, different patches have their own best steps, indicating that a content-aware step controller is needed for optimal image denoising.

reconstructive denoising module is already close to the ground truth, and additional high-frequency details generated by the generative diffusion module may either be unnecessary or even result in artifacts, thereby compromising performance. As depicted in the first row of Figure 3, in a smooth sky region, the direct output of the reconstructive model ($step = 0$) is very similar to the result obtained after 100 iterations of the generative diffusion module, indicating that further generation is unnecessary. Moreover, in the second row, with a 20-step diffusion sampling, it can already recover most of the high-frequency details. Additional details added in the later diffusion sample actually result in artifacts that hurt the visual quality, and the quantitative visual measure (-LPIPS, higher is better) also drops from -0.0653 to -0.0708 when the diffusion step increases from 20 to 100. Only very few patches require a large diffusion step to recover all details, as shown in the third row.

With this observation, it is critical to adaptively determine the diffusion for each low region. Recent work [47] can conveniently traverse the Perception-Distortion curve to achieve different perceptual qualities by manually tuning the different inference steps of the diffusion model, which also proves the possibility of building a control policy of its generation intensity. However, they ignored the demand for refined strength in different texture areas and achieved different perceptual qualities only through manually tuning the inference step, which is infeasible in practice. We consider that different local regions may require different numbers of diffusion steps and design a step controller module to address this issue.

To implement this step controller, we first collect a training dataset by running a trained diffusion model on a large number of image patches, about tens of thousands of image patches. We then conduct a small grid search over the inference step ($step = [0, 10, \dots, 100]$) for every noisy patch and select the best inference step for each patch with minimum LPIPS score [55] (LPIPS measures the perceptual difference between diffusion output and ground truth). The final training pairs consist of input image patches and corresponding ground truth steps for each patch obtained by this searching processing.

We then treat the step prediction as a classification problem. Specifically, we build a lightweight convolution network that is much smaller than reconstructive or generative networks. It consists of eight convolutional blocks, a fully connected layer, and a softmax activation [7], each convolutional block is composed of a 3×3 convolution layer, a batch normalization layer, and a ReLU activation. Maxpooling layers are appended after the second, the fifth, the sixth, and the eighth block respectively. Two residual connections are added: one between the second and fourth layer, and another between the sixth and eighth layer. Finally, we optimize our network using the cross-entropy loss function.

In the inference stage, given the original noisy image, the step controller module will predict a diffusion sampling step number for each local patch, to control the strength of the high-frequency

Algorithm 1 Inference process of the reconstruct-and-generate diffusion model .

Require:

x : noisy image; r_θ : reconstructive model; g_θ : generate model; s_θ : step controller model.

Ensure:

- \hat{y} : detail-preserved denoising result.
 - 1: $\hat{y}_r = r_\theta(x)$; $d_t \sim \mathcal{N}(0, I)$; $T = s_\theta(x)$;
 - 2: **for** $t \leftarrow T$ **to** 1 **do**
 - 3: $\epsilon_t \sim \mathcal{N}(0, I)$; $\gamma_t = \prod_{i=1}^t \alpha_i$;
 - 4: $d_{t-1} \leftarrow \frac{1}{\sqrt{\alpha_t}}(d_t - \frac{1-\alpha_t}{\sqrt{1-\gamma_t}}g_\theta(x, d_t, \gamma_t)) + \sqrt{1 - \alpha_t}\epsilon_t$
 - 5: **end for**
 - 6: **return** $\hat{y} = \hat{y}_r + d_0$
-

detail generation, as shown in Figure 2. Algorithm 1 summarizes the entire inference process of the RnG model.

In most experiments, metrics are only calculated on 256×256 patches. In the case of larger images with resolutions exceeding 256×256 , we divide them into 256×256 patches with 32-pixel overlap and apply the generative component on each patch individually. When stitching the generated results together, we discard the 12 overlapped boundary pixels from each 256×256 patch while retaining the average value of the remaining 8 boundary pixels. Because our diffusion model only generates high-frequency details, no obvious boundary artifacts are not observed. Please refer to our supplementary material for more visual results.

3.3 Training Scheme and Optimization Targets

To train the reconstructive module, we employ the following training target:

$$\mathcal{L}_{\text{Reconstructive}}(\theta) = \mathbb{E} \|y - r_\theta(x)\|_p^p. \quad (4)$$

For the generative module, we use the following formula as the training objective:

$$\mathcal{L}_{\text{Generative}}(\theta) = \mathbb{E} \left\| \epsilon - g_\theta(\sqrt{\gamma_t}(y - r_\theta(x)) + \sqrt{1 - \gamma_t}\epsilon, \gamma_t, x) \right\|_p^p. \quad (5)$$

In the implementation, we choose $p = 2$ for the reconstructive module and $p = 1$ for the generative module.

At last, we introduce the novel two-stage training scheme for the RnG. Specifically, we first use the pixel-loss function to train the reconstructive model. When the reconstructive model converges, we freeze the parameters and then start training the generative model. Unlike most multi-module networks, we did not end-to-end fine-tune both modules together but trained them sequentially instead. This is because as shown by previous research [49; 38], when training a convolutional neural network to fit a function (in this case, it is a denoising function), it often fits the low-frequency component of the function first and fits the high-frequency component in the later training iterations. If the reconstructive module and generative module are jointly optimized, they will interfere with each other and not work as expected. Therefore, it is necessary to train our RnG with the two-stage scheme, letting the diffusion model focus on learning high-frequency details when training the generative module. Our experiments in Section 4.3 also demonstrate that it is crucial to train our RnG by using the two-stage training scheme.

4 Experiments

In this section, we will introduce experiments that verify the effectiveness of the proposed approach.

Dataset. We train and evaluate our models on widely used real and synthetic denoising datasets. For a fair comparison, we follow the same setup used by [12; 51; 31; 57] and evaluate our model on:

- **Real Image Denoising Dataset.** We use the Smartphone Image Denoising Dataset (SIDDD) [1], a widely used real denoising dataset. It consists of images from 10 static scenes under different lighting conditions captured by 5 representative smartphone cameras. There are 320 image pairs for training and 1280 image patch pairs for validation.

Table 1: Experimental results of ablation on training strategy, reconstructive denoising net and generative diffusion condition using SIDD dataset. The combination of the two-stage training scheme, condition with noisy image, and reconstructive module of NAFNet lead to the best settings, which is the framework of the proposed RnG. *Joint Opti.* is short for joint optimization. *Inter. Supv.* stands for intermediate supervision. *Init. Est.* stands for initial estimation.

Training Scheme			Reconstructive Module		Condition		Metric	
Joint Opti.	Inter. Supv.	Two-Stage	U-Net	NAFNet	Noisy	Init. Est.	PSNR \uparrow	LPIPS \downarrow
✓			✓		✓		32.4438	0.1360
	✓		✓		✓		37.2392	0.1185
		✓	✓		✓		36.7467	0.1091
		✓		✓		✓	38.0268	0.1116
		✓		✓	✓		38.1088	0.0997

- Gaussian Image Denoising Dataset.** Following [31; 57], we conduct denoising experiments on several widely-used synthetic color image benchmarks (DIV2K [2] and Flickr2K [50]) with additive white Gaussian noise. Compared with testing benchmark datasets (CBSD68 [34], Kodak24 [20], McMaster [54], Urban100 [24]), DIV2K is more diverse, with 800 training images, 100 validation images, and 100 test images. The training dataset consists of images from both DIV2K and Flickr2K, and the validation dataset consists of images from DIV2K, with synthetic added Gaussian noise with a standard deviation of $\sigma \in [20, 35, 50]$.

Training Details. We employ the state-of-the-art denoising method, NAFNet [12], as our reconstructive denoising module, adopting the same training setup similar to [12]. Specifically, our training data consists of 128×128 randomly cropped patches and we adopt training-time data augmentation with random horizontal/vertical flips and $90^\circ/180^\circ/270^\circ$ rotations, similar to [12], with a batch size of 256. We use the AdamW [32] optimizer with a fixed learning rate of 0.0001, a weight decay rate of 0.0001, and an EMA decay rate of 0.9999. During training, following [41; 47], we use a fine-grained diffusion process with $T = 2000$ steps and use a linear noise schedule with the two endpoints set as: $1 - \alpha_0 = 1 \times 10^{-6}$ and $1 - \alpha_T = 0.01$.

Evaluation Metrics. We evaluate our method on different distortion-based metrics and perceptual metrics: PSNR, SSIM [46], LPIPS [55], NIQE [35]. We use the implementation from the image quality assessment toolbox by [10]² It should be noted that the improvement in distortion accuracy (e.g., PSNR, SSIM) is not always accompanied by an improvement in perceptual quality, which is known as the Perception-Distortion trade-off [6]. Although an increase in perception metric will also lead to a decrease in distortion metric, one would never need to sacrifice more than $3dB$ in PSNR to obtain perfect perceptual quality.

4.1 Results on Real Noise

Table 2 shows denoising results on the real noise dataset, SIDD [1]. We compared our model with four reconstructive-based denoising methods (NAFNet [12], Restormer [51], Cycle-ISP [52], MAXIM [45]), generative-based denoising methods (DDRM [27], LDM [39]) and GAN-based methods (NAFNet with perceptual loss [26], PDASR [56]). Our model achieves the best performance across both perceptual metrics (both LPIPS and NIQE) while there are only minor drops in distortion metrics (PSNR and SSIM). Note that pure generative methods (DDRM and LDM) and GAN-based methods (PDASR) sacrifice more than $5dB$ in PSNR, which results in notable artifacts in the final result. Also, perceptual metrics (LPIPS and NIQE) are more consistent with our visual perception. **Please refer to our supplementary material for more visual comparison.** Furthermore, our approach outperforms diffusion-based techniques by requiring only 76 averaged inference steps to achieve the best results.

4.2 Results on Synthetic Gaussian Noise

Table 3 shows denoising results on synthetic Gaussian noise. For a fair comparison, we train all models only using the synthetic dataset mentioned by Section 4 and test on the same noisy images. Compared with both reconstructive-based denoising methods and generative-based denoising methods, our model achieves considerable perceptual performance while maintaining comparable distortion and

²We use the assessment toolbox provided at <https://github.com/chaofengc/IQA-PyTorch>.

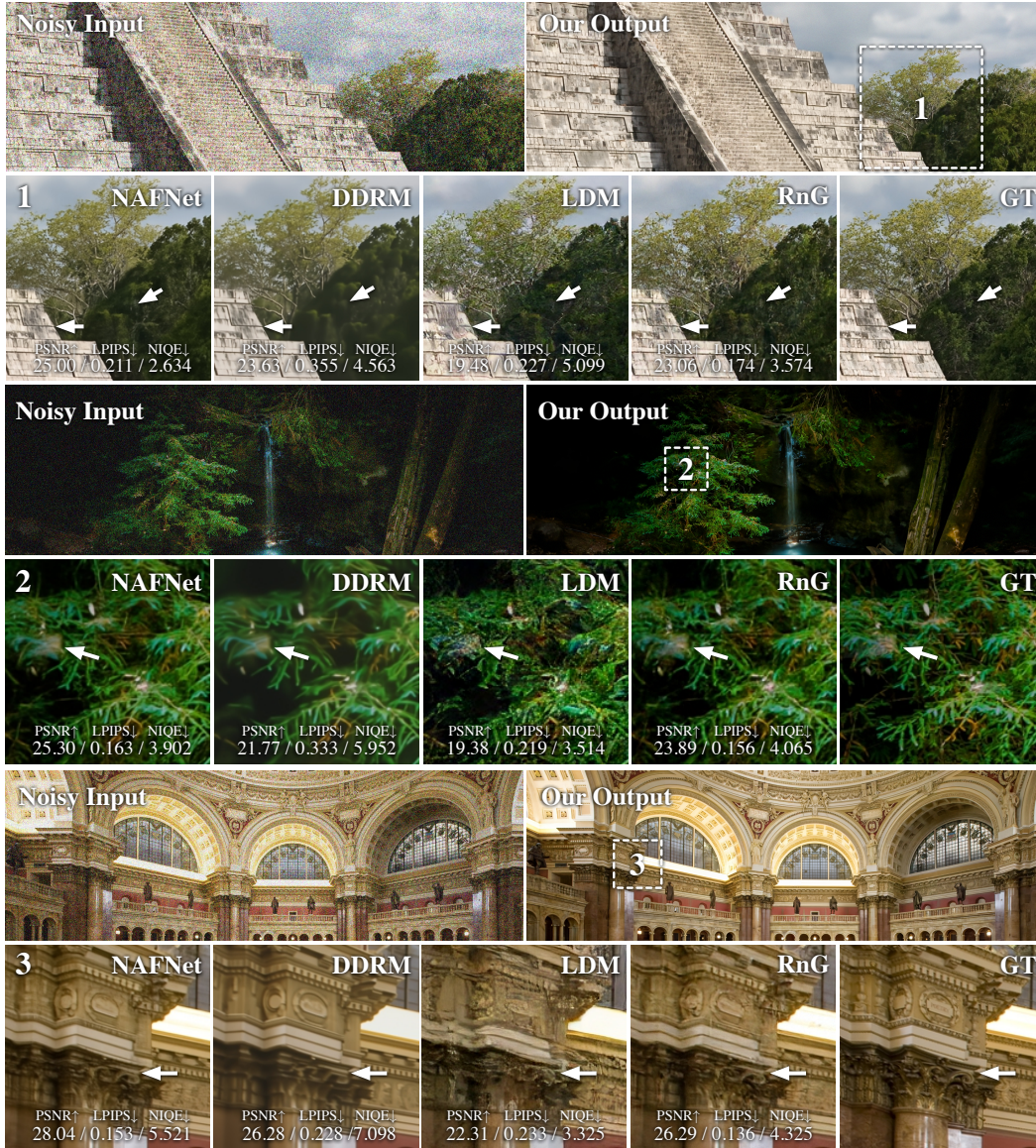


Figure 4: Visual comparison on the DIV2K dataset (zoom-in for a better view). The proposed RnG method preserves more details compared with the reconstructive method (NAFNet). Furthermore, the high-frequency details generated by RnG are closer to the ground truth, compared with pure generative methods (DDRM and LDM). The proposed RnG method also reports the best LPIPS metric. **Please refer to our supplementary material for full-resolution comparison, where differences between different methods are more obvious.**

only needs 18 inference steps. Notably, pure diffusion-based denoising methods are lower than the reconstructed method (NAFNet) in terms of LPIPS perceptual metrics, which illustrates that pure diffusion-based denoising methods are prone to some artifacts. Although LDM achieves a lower NIQE metric, non-reference metrics are not always appropriate.

We further show the qualitative performance of our method in Figure 4. The proposed RnG inherits the advantages of both the fidelity from the reconstructive methods and the detail-preserving ability from the generative methods. By observing numeric and visual results, it can be seen that LPIPS is the perceptual metric that most closely aligns with human perception. For example, in the third scene, while LDM achieves the highest NIQE score, its generated texture is chaotic and far from visually satisfactory. Comparing our results with the NAFNet, it can be found that while the LPIPS is improved, the PSNR will slightly decrease, which corresponds to the perceptual-distortion trade-off.

Table 2: Image denoising results on the SIDD dataset. Our RnG achieves the best LPIPS perceptual metric while maintaining comparable PSNR.

SIDD						
Type	Model	LPIPS↓	NIQE↓	PSNR↑	SSIM↑	Inference Step
N/A	Ground Truth	0.0	10.3890	$+\infty$	1.00	-
Reconstructive	CycleISP	0.2101	16.5107	39.2715	0.9431	-
	MAXIM	0.1895	16.6797	39.6786	0.9469	-
	Restormer	0.1978	16.8028	39.9282	0.9469	-
	NAFNet	0.1877	16.0501	40.2110	0.9496	-
Generative	DDRM	0.2879	18.1422	34.7716	0.9148	200
	LDM	0.0852	13.1519	34.7656	0.9004	200
Both	NAFNet (with perceptual loss)	0.1790	16.2380	39.6472	0.9457	-
	PDASR(with GAN loss, P-D trade-off)	0.1298	12.1099	34.9306	0.9194	-
	RnG (Ours)	0.0719	11.8473	38.0291	0.9256	76

Table 3: Image denoising results on the DIV2K dataset. Our RnG achieves the best LPIPS perceptual metric while maintaining comparable PSNR.

DIV2K						
Type	Model	LPIPS↓	NIQE↓	PSNR↑	SSIM↑	Inference Step
N/A	Ground Truth	0.0	7.9515	$+\infty$	1.00	-
Reconstructive	NAFNet	0.1308	10.6393	33.1860	0.8883	-
Generative	DDRM	0.1826	12.4311	30.4951	0.8484	200
	LDM	0.1656	8.6438	26.8525	0.7251	200
Both	RnG (Ours)	0.1040	9.1549	31.6678	0.8603	18

4.3 Ablation Study and Analysis

Framework. To further illustrate the effectiveness of our framework, we conduct ablation experiments from three aspects: the training schemes, the initial denoising network, and the conditional input of the diffusion model. In terms of training strategies, three main strategies are mainly compared: joint training, intermediate supervised training, and two-stage training. In terms of the initial denoising network, we compared U-Net with NAFNet [12] we currently used. In addition, we also explored the conditional input of the diffusion model using noisy images compared to the initial estimation result.

In Table 1, we start from a simple U-Net architecture baseline, similar to [47], and gradually enable each of the aforementioned settings. All models are trained for 1M steps to ensure that the differences are not due to insufficient training. During the inference, we use 500 steps with a linear noise schedule, similar to [47]. Through a detailed ablation study, we find that this setting reports the best performance: using a two-stage training scheme, the NAFNet as the reconstructive module, and the original noisy image as the conditional input of the diffusion model. This result proves the rationality of the framework design of the proposed RnG.

In addition, we compare our RnG with the reconstructive part only and the generative part only to show the effectiveness and plausibility of our designed framework. During inference, we use 2,000 steps with a linear noise schedule, similar to [41]. As shown in Table 4, the reconstructive part only achieves the best distortion metric with lower perception, the generative part only can achieve good perception but cannot guarantee fidelity (lower PSNR), while our method can balance fidelity and perceptual quality, and achieve the best perceptual performance. More visual results can be found in Figure 6. Our RnG can combine the advantages of reconstruction and generation to achieve a balance of perception and distortion.

What the Generative Part Learns. We visualize the output of the generative part of the proposed RnG model on the DIV2K dataset to analyze what the generative part learns. Figure 5 shows that the residual detail information generated at each step within the diffusion model encompasses mainly high-frequency texture.

Step Controller. At last, we conduct an ablation study to demonstrate the effectiveness of the step controller module. Table 5 shows that our step controller module can bring significant improvements

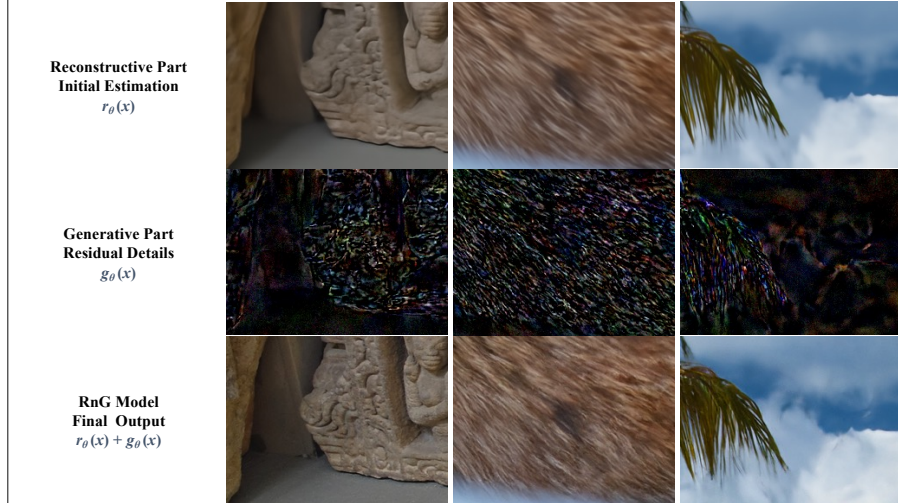


Figure 5: The visualization of the high-frequency residual details produced by the generative part. The initial estimations produced by the reconstructive part as well as the final outputs of the RnG model are also presented. The generative part effectively brings more high-frequency details to the over-smoothed reconstructive output, achieving higher perceptual quality.



Figure 6: Visualization results of different components in reconstruct-and-generate diffusion model. We see that the reconstructive model predicts smooth results, the generative model predicts artifacts, and our RnG achieves better visual quality.

in both distortion and perception quality under the same inference step. These improvements demonstrate the importance of the step controller module. As shown in Figure 3, different texture regions have different requirements for steps, flat regions require fewer steps and textured regions require more steps.

Table 4: Experimental results of ablation on components in RnG using SIDD dataset. Our RnG achieves the best perceptual metric while maintaining comparable PSNR.

Model	LPIPS↓	PSNR↑
Reconstructive Part Only	0.1877	40.2110
Generative Part Only	0.0934	35.8663
Ours (w/o step controller)	0.0891	37.8497

Table 5: Experimental results of ablation on step controller module using DIV2K dataset. Our method with a step controller module significantly outperforms our method with a fixed step under both perceptual and distortion metrics.

Step Controller	LPIPS↓	PSNR↑
	0.1078	31.0144
✓	0.1040	31.6678

5 Conclusion

In this paper, we combined the strengths of reconstruction and generation methods and presented the RnG diffusion model for image denoising, which focuses on pursuing a better balance between perception and distortion. We further introduced a step controller to improve the perceptual quality of RnG and eliminate unnecessary computation costs. Our experimental results show that our method significantly improves perceptual quality compared to the current state-of-the-art methods while maintaining reasonable distortion quality. In future work, we would focus on reducing the computational complexity of the proposed methods since their computational cost is still expensive for edge devices, which is also a common problem of diffusion-based approaches.

References

- [1] Abdelrahman Abdelhamed, Stephen Lin, and Michael S Brown. A high-quality denoising dataset for smartphone cameras. In *Proceedings of the IEEE conference on computer vision and pattern recognition*, pages 1692–1700, 2018.
- [2] Eirikur Agustsson and Radu Timofte. Ntire 2017 challenge on single image super-resolution: Dataset and study. In *Proceedings of the IEEE conference on computer vision and pattern recognition workshops*, pages 126–135, 2017.
- [3] Michal Aharon, Michael Elad, and Alfred Bruckstein. K-svd: An algorithm for designing overcomplete dictionaries for sparse representation. *IEEE Transactions on signal processing*, 54(11):4311–4322, 2006.
- [4] Abeer Alsaiani, Ridhi Rustagi, Manu Mathew Thomas, Angus G Forbes, et al. Image denoising using a generative adversarial network. In *2019 IEEE 2nd international conference on information and computer technologies (ICICT)*, pages 126–132. IEEE, 2019.
- [5] Joshua Batson and Loic Royer. Noise2self: Blind denoising by self-supervision. In *International Conference on Machine Learning*, pages 524–533. PMLR, 2019.
- [6] Yochai Blau and Tomer Michaeli. The perception-distortion tradeoff. In *Proceedings of the IEEE conference on computer vision and pattern recognition*, pages 6228–6237, 2018.
- [7] John Bridle. Training stochastic model recognition algorithms as networks can lead to maximum mutual information estimation of parameters. *Advances in neural information processing systems*, 2, 1989.
- [8] Antoni Buades, Bartomeu Coll, and J-M Morel. A non-local algorithm for image denoising. In *2005 IEEE computer society conference on computer vision and pattern recognition (CVPR'05)*, volume 2, pages 60–65. Ieee, 2005.
- [9] Sungmin Cha, Taeon Park, and Taesup Moon. Gan2gan: Generative noise learning for blind image denoising with single noisy images. *arXiv preprint arXiv:1905.10488*, 3, 2019.
- [10] Chaofeng Chen and Jiadi Mo. IQA-PyTorch: Pytorch toolbox for image quality assessment. [Online]. Available: <https://github.com/chaofengc/IQA-PyTorch>, 2022.
- [11] Jingwen Chen, Jiawei Chen, Hongyang Chao, and Ming Yang. Image blind denoising with generative adversarial network based noise modeling. In *Proceedings of the IEEE conference on computer vision and pattern recognition*, pages 3155–3164, 2018.
- [12] Liangyu Chen, Xiaojie Chu, Xiangyu Zhang, and Jian Sun. Simple baselines for image restoration. In *Computer Vision—ECCV 2022: 17th European Conference, Tel Aviv, Israel, October 23–27, 2022, Proceedings, Part VII*, pages 17–33. Springer, 2022.
- [13] Nanxin Chen, Yu Zhang, Heiga Zen, Ron J Weiss, Mohammad Norouzi, and William Chan. Wavegrad: Estimating gradients for waveform generation. *arXiv preprint arXiv:2009.00713*, 2020.
- [14] Kostadin Dabov, Alessandro Foi, Vladimir Katkovnik, and Karen Egiazarian. Image denoising by sparse 3-d transform-domain collaborative filtering. *IEEE Transactions on image processing*, 16(8):2080–2095, 2007.
- [15] Kostadin Dabov, Alessandro Foi, Vladimir Katkovnik, and Karen Egiazarian. Image restoration by sparse 3d transform-domain collaborative filtering. In *Image Processing: Algorithms and Systems VI*, volume 6812, pages 62–73. SPIE, 2008.
- [16] Nithish Divakar and R Venkatesh Babu. Image denoising via cnns: An adversarial approach. In *Proceedings of the IEEE Conference on Computer Vision and Pattern Recognition Workshops*, pages 80–87, 2017.
- [17] Weisheng Dong, Xin Li, Lei Zhang, and Guangming Shi. Sparsity-based image denoising via dictionary learning and structural clustering. In *CVPR 2011*, pages 457–464. IEEE, 2011.

- [18] Weisheng Dong, Guangming Shi, and Xin Li. Nonlocal image restoration with bilateral variance estimation: a low-rank approach. *IEEE transactions on image processing*, 22(2):700–711, 2012.
- [19] Michael Elad and Michal Aharon. Image denoising via sparse and redundant representations over learned dictionaries. *IEEE Transactions on Image processing*, 15(12):3736–3745, 2006.
- [20] Rich Franzen. Kodak lossless true color image suite. *source: <http://r0k.us/graphics/kodak>*, 4(2), 1999.
- [21] Ian Goodfellow, Jean Pouget-Abadie, Mehdi Mirza, Bing Xu, David Warde-Farley, Sherjil Ozair, Aaron Courville, and Yoshua Bengio. Generative adversarial networks. *Communications of the ACM*, 63(11):139–144, 2020.
- [22] Shuhang Gu, Lei Zhang, Wangmeng Zuo, and Xiangchu Feng. Weighted nuclear norm minimization with application to image denoising. In *Proceedings of the IEEE conference on computer vision and pattern recognition*, pages 2862–2869, 2014.
- [23] Jonathan Ho, Ajay Jain, and Pieter Abbeel. Denoising diffusion probabilistic models. *Advances in Neural Information Processing Systems*, 33:6840–6851, 2020.
- [24] Jia-Bin Huang, Abhishek Singh, and Narendra Ahuja. Single image super-resolution from transformed self-exemplars. In *Proceedings of the IEEE conference on computer vision and pattern recognition*, pages 5197–5206, 2015.
- [25] Viren Jain and Sebastian Seung. Natural image denoising with convolutional networks. *Advances in neural information processing systems*, 21, 2008.
- [26] Justin Johnson, Alexandre Alahi, and Li Fei-Fei. Perceptual losses for real-time style transfer and super-resolution. In *Computer Vision—ECCV 2016: 14th European Conference, Amsterdam, The Netherlands, October 11–14, 2016, Proceedings, Part II 14*, pages 694–711. Springer, 2016.
- [27] Bahjat Kawar, Michael Elad, Stefano Ermon, and Jiaming Song. Denoising diffusion restoration models. *arXiv preprint arXiv:2201.11793*, 2022.
- [28] Bahjat Kawar, Gregory Vaksman, and Michael Elad. Stochastic image denoising by sampling from the posterior distribution. In *Proceedings of the IEEE/CVF International Conference on Computer Vision*, pages 1866–1875, 2021.
- [29] Alexander Krull, Tim-Oliver Buchholz, and Florian Jug. Noise2void-learning denoising from single noisy images. In *Proceedings of the IEEE/CVF conference on computer vision and pattern recognition*, pages 2129–2137, 2019.
- [30] Jaakko Lehtinen, Jacob Munkberg, Jon Hasselgren, Samuli Laine, Tero Karras, Miika Aittala, and Timo Aila. Noise2noise: Learning image restoration without clean data. *arXiv preprint arXiv:1803.04189*, 2018.
- [31] Jingyun Liang, Jiezhong Cao, Guolei Sun, Kai Zhang, Luc Van Gool, and Radu Timofte. Swinir: Image restoration using swin transformer. In *Proceedings of the IEEE/CVF international conference on computer vision*, pages 1833–1844, 2021.
- [32] Ilya Loshchilov and Frank Hutter. Decoupled weight decay regularization. *arXiv preprint arXiv:1711.05101*, 2017.
- [33] Andreas Lugmayr, Martin Danelljan, and Radu Timofte. Ntire 2021 learning the super-resolution space challenge. In *Proceedings of the IEEE/CVF Conference on Computer Vision and Pattern Recognition*, pages 596–612, 2021.
- [34] David Martin, Charless Fowlkes, Doron Tal, and Jitendra Malik. A database of human segmented natural images and its application to evaluating segmentation algorithms and measuring ecological statistics. In *Proceedings Eighth IEEE International Conference on Computer Vision. ICCV 2001*, volume 2, pages 416–423. IEEE, 2001.
- [35] Anish Mittal, Rajiv Soundararajan, and Alan C Bovik. Making a “completely blind” image quality analyzer. *IEEE Signal processing letters*, 20(3):209–212, 2012.

- [36] Tongyao Pang, Huan Zheng, Yuhui Quan, and Hui Ji. Recorrupted-to-recorrupted: unsupervised deep learning for image denoising. In *Proceedings of the IEEE/CVF conference on computer vision and pattern recognition*, pages 2043–2052, 2021.
- [37] Yuhui Quan, Mingqin Chen, Tongyao Pang, and Hui Ji. Self2self with dropout: Learning self-supervised denoising from single image. In *Proceedings of the IEEE/CVF conference on computer vision and pattern recognition*, pages 1890–1898, 2020.
- [38] Nasim Rahaman, Aristide Baratin, Devansh Arpit, Felix Draxler, Min Lin, Fred Hamprecht, Yoshua Bengio, and Aaron Courville. On the spectral bias of neural networks. In *International Conference on Machine Learning*, pages 5301–5310. PMLR, 2019.
- [39] Robin Rombach, Andreas Blattmann, Dominik Lorenz, Patrick Esser, and Björn Ommer. High-resolution image synthesis with latent diffusion models. In *Proceedings of the IEEE/CVF Conference on Computer Vision and Pattern Recognition*, pages 10684–10695, 2022.
- [40] Chitwan Saharia, William Chan, Huiwen Chang, Chris Lee, Jonathan Ho, Tim Salimans, David Fleet, and Mohammad Norouzi. Palette: Image-to-image diffusion models. In *ACM SIGGRAPH 2022 Conference Proceedings*, pages 1–10, 2022.
- [41] Chitwan Saharia, Jonathan Ho, William Chan, Tim Salimans, David J Fleet, and Mohammad Norouzi. Image super-resolution via iterative refinement. *IEEE Transactions on Pattern Analysis and Machine Intelligence*, 2022.
- [42] Jascha Sohl-Dickstein, Eric Weiss, Niru Maheswaranathan, and Surya Ganguli. Deep unsupervised learning using nonequilibrium thermodynamics. In *International Conference on Machine Learning*, pages 2256–2265. PMLR, 2015.
- [43] Yang Song and Stefano Ermon. Generative modeling by estimating gradients of the data distribution. *Advances in neural information processing systems*, 32, 2019.
- [44] Yang Song, Jascha Sohl-Dickstein, Diederik P Kingma, Abhishek Kumar, Stefano Ermon, and Ben Poole. Score-based generative modeling through stochastic differential equations. *arXiv preprint arXiv:2011.13456*, 2020.
- [45] Zhengzhong Tu, Hossein Talebi, Han Zhang, Feng Yang, Peyman Milanfar, Alan Bovik, and Yinxiao Li. Maxim: Multi-axis mlp for image processing. In *Proceedings of the IEEE/CVF Conference on Computer Vision and Pattern Recognition*, pages 5769–5780, 2022.
- [46] Zhou Wang, Alan C Bovik, Hamid R Sheikh, and Eero P Simoncelli. Image quality assessment: from error visibility to structural similarity. *IEEE transactions on image processing*, 13(4):600–612, 2004.
- [47] Jay Whang, Mauricio Delbracio, Hossein Talebi, Chitwan Saharia, Alexandros G Dimakis, and Peyman Milanfar. Deblurring via stochastic refinement. In *Proceedings of the IEEE/CVF Conference on Computer Vision and Pattern Recognition*, pages 16293–16303, 2022.
- [48] Jun Xu, Yuan Huang, Ming-Ming Cheng, Li Liu, Fan Zhu, Zhou Xu, and Ling Shao. Noisy-as-clean: Learning self-supervised denoising from corrupted image. *IEEE Transactions on Image Processing*, 29:9316–9329, 2020.
- [49] Zhi-Qin John Xu, Yaoyu Zhang, Tao Luo, Yanyang Xiao, and Zheng Ma. Frequency principle: Fourier analysis sheds light on deep neural networks. *arXiv preprint arXiv:1901.06523*, 2019.
- [50] Peter Young, Alice Lai, Micah Hodosh, and Julia Hockenmaier. From image descriptions to visual denotations: New similarity metrics for semantic inference over event descriptions. *Transactions of the Association for Computational Linguistics*, 2:67–78, 2014.
- [51] Syed Waqas Zamir, Aditya Arora, Salman Khan, Munawar Hayat, Fahad Shahbaz Khan, and Ming-Hsuan Yang. Restormer: Efficient transformer for high-resolution image restoration. In *Proceedings of the IEEE/CVF Conference on Computer Vision and Pattern Recognition*, pages 5728–5739, 2022.

- [52] Syed Waqas Zamir, Aditya Arora, Salman Khan, Munawar Hayat, Fahad Shahbaz Khan, Ming-Hsuan Yang, and Ling Shao. Cycleisp: Real image restoration via improved data synthesis. In *Proceedings of the IEEE/CVF conference on computer vision and pattern recognition*, pages 2696–2705, 2020.
- [53] Kai Zhang, Wangmeng Zuo, Yunjin Chen, Deyu Meng, and Lei Zhang. Beyond a gaussian denoiser: Residual learning of deep cnn for image denoising. *IEEE transactions on image processing*, 26(7):3142–3155, 2017.
- [54] Lei Zhang, Xiaolin Wu, Antoni Buades, and Xin Li. Color demosaicking by local directional interpolation and nonlocal adaptive thresholding. *Journal of Electronic imaging*, 20(2):023016–023016, 2011.
- [55] Richard Zhang, Phillip Isola, Alexei A Efros, Eli Shechtman, and Oliver Wang. The unreasonable effectiveness of deep features as a perceptual metric. In *Proceedings of the IEEE conference on computer vision and pattern recognition*, pages 586–595, 2018.
- [56] Yuehan Zhang, Bo Ji, Jia Hao, and Angela Yao. Perception-distortion balanced admm optimization for single-image super-resolution. In *European Conference on Computer Vision*, pages 108–125. Springer, 2022.
- [57] Yulun Zhang, Yapeng Tian, Yu Kong, Bineng Zhong, and Yun Fu. Residual dense network for image super-resolution. In *Proceedings of the IEEE conference on computer vision and pattern recognition*, pages 2472–2481, 2018.